Available online at www.sciencedirect.com

ScienceDirect

Physics Procedia 83 (2016) 1013 – 1020

Physics Procedia

9th International Conference on Photonic Technologies - LANE 2016

Time-resolved visualization of laser beam melting of silica glass powder

I. Zhirnov[a], R.S. Khmyrov[a], C.E. Protasov[a], A.V. Gusarov[a,b,*]

[a]*Moscow State University of Technology "STANKIN", Vadkovsky per. 3a, 127055 Moscow, Russia*
[b]*Institute of Photonic Technologies (LPT),Friedrich-Alexander-Universität Erlangen-Nürnberg, Konrad-Zuse-Str.3-5, 91052 Erlangen, Germany*

Abstract

Silica glass is an inorganic dielectric material that can be used for laser beam melting without cracking. However, the extremely high viscosity makes consolidation of powder very slow. To study the dynamics of consolidation, a 10.6 μm laser beam was directed on the powder layer deposited on the solid substrate of the same material. The laser-interaction zone was lighted with green laser and filmed with a high-speed camera at 6000 fps. The process develops steadily. Neither fluctuation nor droplets are observed. An expanding consolidation zone is observed. Viscous merging of softened powder particles is supposed to be the principal mechanism of consolidation. Mathematical model based on this mechanism confirms formation of the consolidated zone in the center. Both the experiment and the model indicate that consolidation looks like propagation of a sharp front. Comparison of the experiments and the calculations estimates the consolidation front temperature of about 1800-1900 K.

Peer-review under responsibility of the Bayerisches Laserzentrum GmbH

Keywords: high-speed camera; powder consolidation; schrinkage; modeling; heat transfer

1. Introduction

The majority of ceramics and glasses are difficult to process by laser. The examples for laser beam melting (LBM) of alumina and zirconia are shown in the works by Deckers et al. (2014) and Li et al. (2014), respectively. The principal problem is cracking. Optimizing the laser parameters is not effective to reduce cracking. The cited works have proven that only uniform preheating of the laser-treated body is useful. Indeed, the preheating

* Corresponding author. Tel.: +49-9131-85-23241 .
E-mail address: av.goussarov@gmail.com

Peer-review under responsibility of the Bayerisches Laserzentrum GmbH
doi:10.1016/j.phpro.2016.08.106

considerably reduced cracking but could not completely eliminate it. The reason is that laser beam locally heats the treated material and thus gives rise to a thermal shock. Inorganic dielectrics are brittle and often not resistant to thermal shocks. Thermomechanical simulation of laser processing by Gusarov et al. (2011, 2013) indicated that the residual stresses are proportional to the difference between the melting (softening) and the ambient temperatures. This justifies the preheating. Another way is to choose a material with high elasticity-to-thermal expansion ratio.

Silica glass is well known by its resistance to thermal shocks due to extremely low thermal expansion. Indeed, it was successfully applied for LBM by Tang et al. (2006) and Khmyrov et al. (2016). The material was not cracked even without preheating. Silica glass combines high corrosion resistance and dielectric strength with high-temperature mechanical strength. Therefore, layer-by-layer additive manufacturing by LBM of silica glass powder is promising. However, the quality of the obtained material was shown to be very sensitive to the process parameters. This is because of slow consolidation of silica glass powder controlled by its extremely high viscosity. The window of the optimal process parameters for silica glass is considerably narrower than that for some metal alloys widely used in LBM. This is because the temperature in the zone of laser action should be as high as possible to attain satisfactory consolidation rate and, on the other hand, the excessive laser power gives rise to undesirable evaporation.

Time-resolved visualization is known to be useful for studying LBM of metal alloys. For example, Okunkova et al. (2014) revealed important details of powder consolidation and gave useful recommendation for the process optimization. This technique has not been applied to silica glass yet. However, optimization of silica glass LBM is more difficult. The objective of the present work is to study the consolidation kinetics of silica glass powder at LBM with a high-speed camera.

2. Materials and experimental methods

Samples for LBM were prepared by depositing 20-μm silica glass powder on a 5 mm-thick plate of the same material. The powder layer thickness varied from 70 to 100 μm. The experimental details of the LBM process and the setup with CO_2 laser source were described by Khmyrov et al. (2016). The principal process parameters were 24 W laser power, 1.5 mm laser spot diameter, and zero scanning speed. The process was filmed with high-speed CCD camera Photron SA5. To exclude the influence of reflected laser beam on the CCD camera, pulsed diode laser lighting source Cavilux with a wavelength of 800 nm and an optical filter were used. The camera and the lighting source were mounted opposite to each other at the angle of 45 degrees to the sample as shown in Fig. 1. The frame rate was set to 6000 fps and the exposure was 166.42 μs. The pulsed diode lighting was synchronized with the camera. An 8-fold magnification Macro lens was used for higher spatial resolution. The image resolution was 1024x1024 pixels. The surface of several samples was covered with an aniline ink to improve contrast.

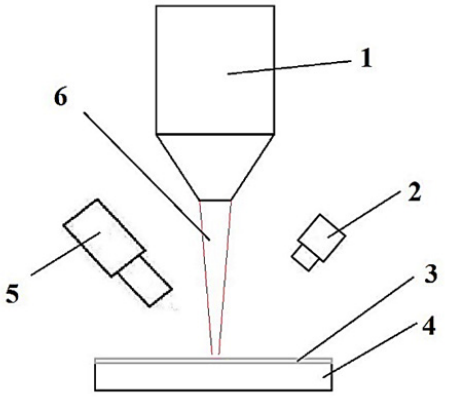

Fig. 1. Experimental setup for visualization of the LBM process: CO_2 laser head (1); pulsed diode laser lighting source (2); powder layer (3); silica glass substrate (4); CCD camera (5); laser beam (6).

3. Experimental results

The obtained films of the process show steadily developing images. Neither fluctuation nor droplets were observed. The evolution of the laser-interaction zone can be represented by the set of frames shown in Fig. 2. Visual investigation of the sample after the process indicates a depression zone. The diameter of the depression zone approximately corresponds to the contrast circle in Fig. 2. The depression may arise due to shrinkage of powder at consolidation. Optical microscopy (see Fig. 3) show a dark zone in the center. This zone indicates low scattering of light. Light can be scattered by the surfaces of powder particles and the substrate. Thus, the powder is likely to be consolidated and fused with the substrate within the dark zone in Fig. 3. Figure 4 shows laser processing of powder colored with ink. An expanding dark ring is clearly visible. The contrast can arise because of thermal decomposition of organic components.

4. Modeling

The experimentally obtained images give qualitative information about powder consolidation kinetics related with the transient temperature field. They can be compared with calculations. The softened particles of quartz glass behave like the droplets of viscous liquid. They tend to coalesce as shown in Fig. 5. The extent of coalescence is characterized by the neck radius a. The kinetics of neck growth between two particles of radius R is estimated by Kingery (1960) as

$$\frac{\mathrm{d}\xi^2}{\mathrm{d}t} = \frac{3}{2}\frac{\sigma}{\eta R} \tag{1}$$

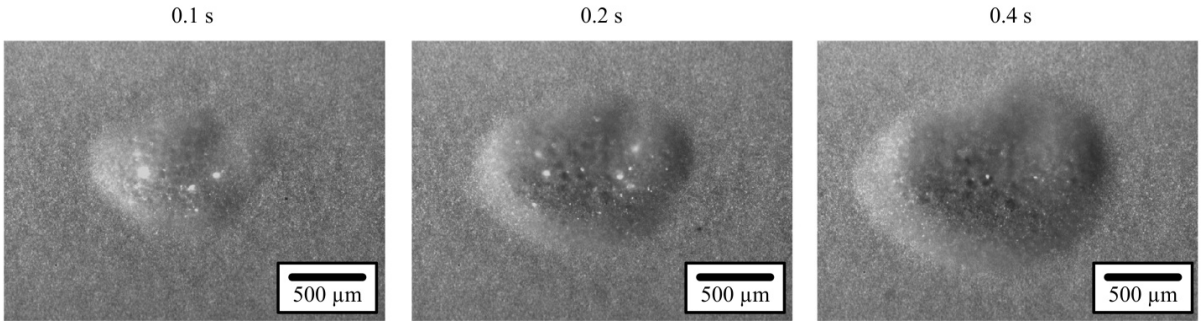

Fig. 2. Laser-interaction zone at SLM. The powder layer thickness is 70 µm. The time after laser turning on is indicated above the frames.

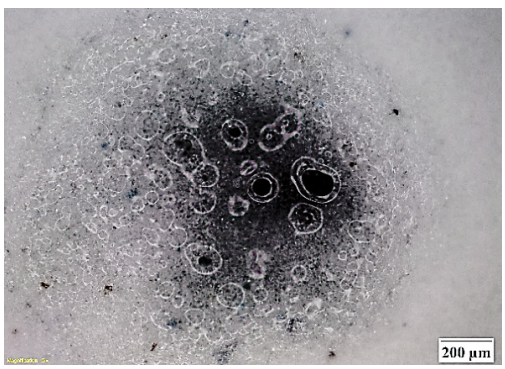

Fig. 3. Microscopic image of the zone of laser impact after laser treatment.

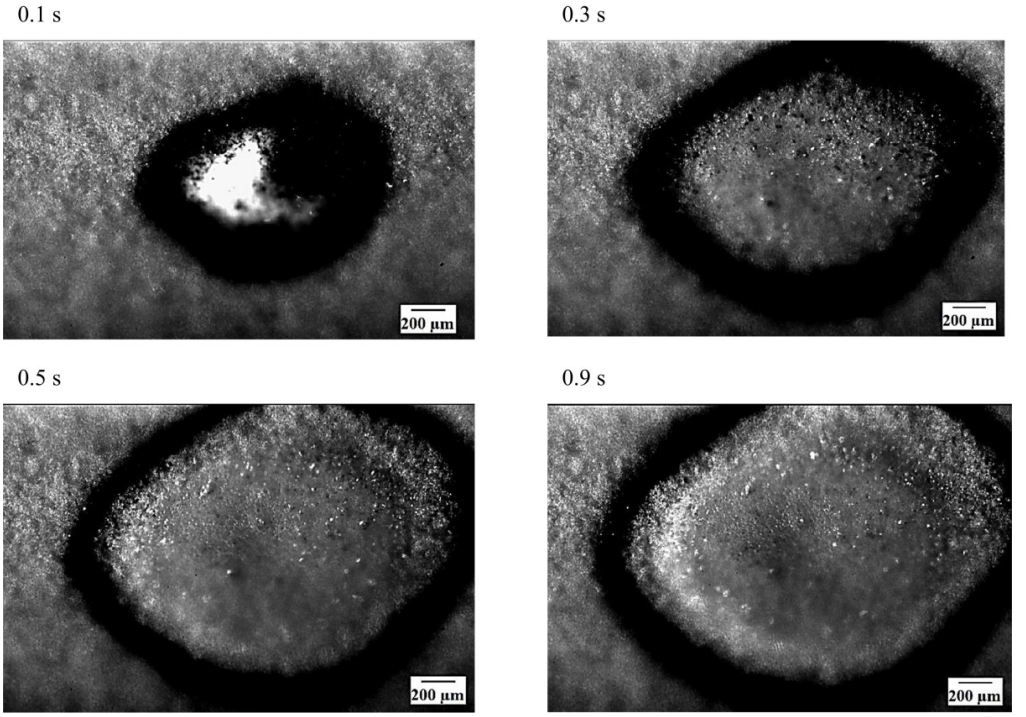

Fig. 4. Laser melting of silica glass powder colored with ink. The powder layer thickness is 100 µm. The time after laser turning on is indicated above the frames.

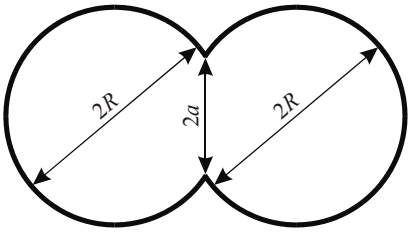

Fig. 5. Coalescence of two spherical particles of radius R with formation of a neck of radius a.

where $\xi = a/R$ is the relative neck radius characterizing the degree of consolidation, t the time, σ the surface tension coefficient, and η the dynamic viscosity. The surface tension coefficient of quartz glass does not considerably vary with temperature and equals about $\sigma = 0.4$ N/m. On the contrary, the viscosity strongly decreases with temperature. Experimental data in the temperature interval up to 1600 K are analyzed by Richter (2006). The approximating curve (curve 1) is plotted in Fig. 6. At temperature above 1600 K, the viscosity is estimated by the extrapolating line (line 2 in Fig. 6).

The temperature field in the laser treated sample is calculated in a Cartesian frame with Z-axis normal to the sample surface by numerical solution of the following heat transfer equation:

$$\frac{\partial H}{\partial t} = \nabla \cdot (\lambda \nabla T), \tag{2}$$

where H is the enthalpy, T the temperature, ∇ the operator nabla, and λ the thermal conductivity. Function $H(T)$

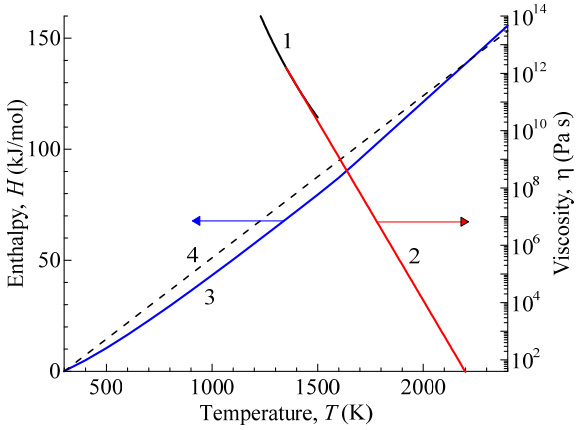

Fig. 6. Parameters for modeling: dynamic viscosity η (1 and 2) and enthalpy H (3 and 4) of silica glass versus temperature T.

reported by JANAF (2016) is shown as curve 3 in Fig. 6. Approximating line 4 is accepted for calculations in this work. Boundary conditions are defined by the energy density flux on the surface due to absorption of the laser beam

$$q_0 = \frac{P_0}{\pi r_0^2} \exp\left(-r^2 / r_0^2\right), \tag{3}$$

where P_0 is the absorbed energy of the laser beam, r_0 its nominal radius, and $r^2 = x^2 + y^2$, and the conditions of strong evaporation are described by Khmyrov et al. (2014).

The thermal conductivity of the powder bed λ is estimated as the sum

$$\lambda = \lambda_{cs} + \lambda_{cg}\,, \tag{4}$$

of conductivity through necks between the powder particles λ_{cs}, and conductivity through gas phase surrounding the particles λ_{cg}. The thermal conductivity through necks is estimated by Gusarov and Kovalev (2009) as

$$\lambda_{cs} = \lambda_s \frac{(1-\varepsilon)N}{\pi} \xi\,, \tag{5}$$

where λ_s is the thermal conductivity of the solid phase, ε the porosity, and N the mean coordination number. The thermal conductivity through the gas phase

$$\lambda_{cg} = F\,\lambda_g\,, \tag{6}$$

is proportional to the gas conductivity λ_g according to Gusarov and Kovalev (2009). The analysis of experimental data indicates that this factor varies from 5 to 7 for particles of diameter about 20 μm packed with porosity 40-50%.

The parameters used for modeling are listed in Table 1. The calculated distribution of temperature T and degree of powder consolidation ξ are shown in Figs. 7-9. The modeling shows the dynamics of expansion of the high-temperature region in the laser-interaction zone. The viscosity of silica glass sharply decreases with temperature. Therefore, calculated degree of consolidation ξ increases in the center up to the values about one, which indicates complete consolidation. Then, the zone of completely consolidated powder expands over the powder layer following to the expansion of the temperature distribution. Distributions of ξ in Figs. 7 and 9 shows that at time $t > 0.1$ s the domain of consolidated powder attains the substrate surface and its lateral boundary becomes sharp. Therefore, according to the modeling, a consolidation front propagates over the powder.

Table 1. Parameters for modeling heat transfer and powder consolidation.

Parameter	Value	Parameter	Value
Particle diameter, R	20 μm	Absorbed laser powder, P_0	24 W
Porosity, ε	0.4	Laser spot radius, r_0	0.75 mm
Gas-phase factor, F	6	Silica glass thermal conductivity, λ_s	2.2 W(m K)
Surface tension, σ	0.4 N/m	Air thermal conductivity, λ_g	$0.0244\frac{W}{m\,K}\left(\frac{T}{273\,\mathrm{K}}\right)^{0.82}$

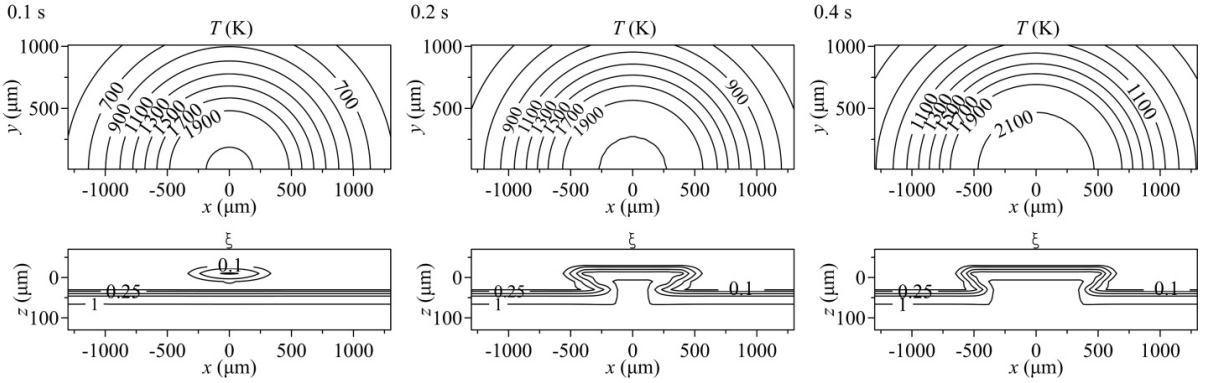

Fig. 7. Calculated distributions of temperature T on the surface of the sample (top row) and degree of consolidation ξ in an axial cross-section (bottom row). The powder layer thickness is 70 μm.

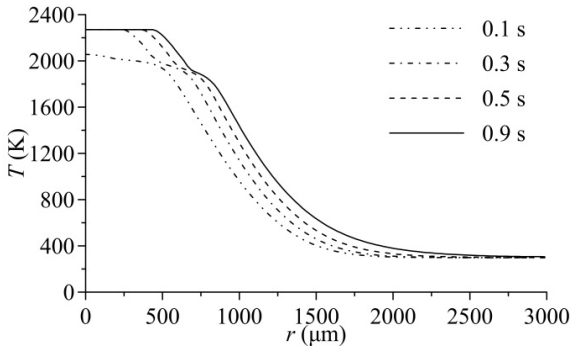

Fig. 8. Calculated radial temperature distributions on the surface of the sample. The powder layer thickness is 100 μm.

5. Discussion

In the experimental images of Fig. 4 at t = 0.5 s and t = 0.9 s, one can distinguish three types of contrast: the zone of smooth surface in the center, the dark ring around it, and the zones of rough surface outside the dark ring and between the ring and the central smooth region. It is expected that the zone of smooth surface corresponds to the consolidated powder. The diameter of this zone D_m is plotted versus time t in Fig. 10. The diameter of the consolidated zone can also be derived from the calculated distributions of Fig. 9 as the maximal diameter $D_{0.5}$ of contour ξ = 0.5 above the substrate surface. The temporal evolution of $D_{0.5}$ is potted in Fig. 10 as well. The calculated diameter of the consolidated zone $D_{0.5}$ underestimates the experimentally observed diameter D_m. The least certain

data for modelling are the viscosity of silica glass extrapolated at high temperatures (see Fig. 6). This uncertainty

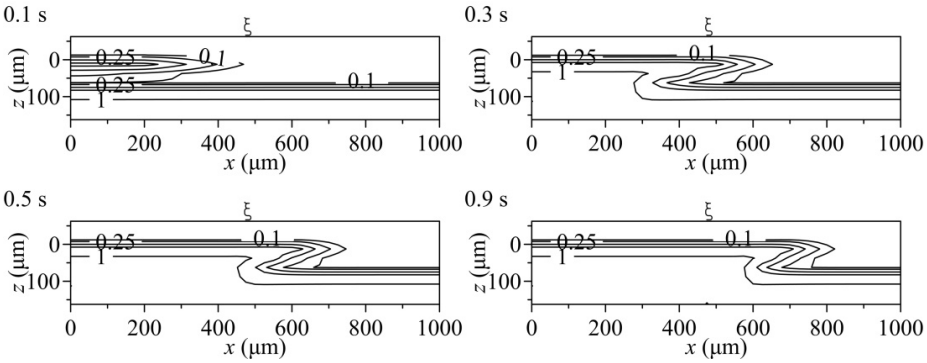

Fig. 9. Calculated distributions of degree of consolidation ξ in an axial cross-section. The powder layer thickness is 100 μm.

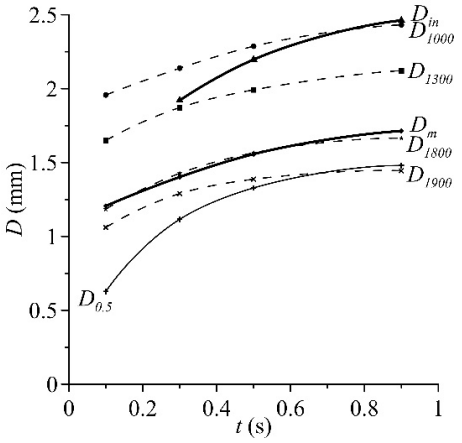

Fig. 10. Characteristic dimensions versus laser exposure time t: experimentally observed diameter of the consolidated zone D_m; experimentally observed inner diameter of the dark ring; calculated diameter of the consolidated zone $D_{0.5}$; calculated diameters of isotherms D_{1000}, D_{1300}, D_{1800}, and D_{1900}.

can explain the difference between calculated $D_{0.5}$ and observed D_m. Calculated diameter D_{1800} of the surface isotherm T = 1800 K is shown by a broken line in Fig. 10. The curve of $D_{1800}(t)$ is very close to curve $D_m(t)$ while the diameter of 1900 K-isotherm $D_{1900}(t)$ is close to the calculated diameter of the consolidated zone $D_{0.5}(t)$. Thus, the temperature of powder consolidation appears to be about 1800-1900 K.

The outer and the inner diameters of the dark ring in Fig. 4 correspond to some transformations with the ink covering the sample surface. The outer boundary may indicate chemical decomposition of the ink while the inner boundary may indicate evaporation of the decomposition products. The both processes are thermally activated, so that expansion of the boundaries reflects expansion of the temperature field. Figure 10 compares experimentally observed inner diameter of the dark ring D_{in} with isotherms T = 1000 K and T = 1300 K. It follows that the inner ring boundary visualizes the surface zone with the temperature about 1000 K to 1300 K.

6. Conclusion

Laser beam melting of silica glass powder is recorded with a high-speed camera at 6000 fps. The process appears to develop steadily. Neither fluctuation nor droplets are observed. An expanding depression zone with smoother surface is formed in the center of the laser-interaction zone. The optical microscopic image of this zone shows dark contrast indicating considerable decrease of light scattering. This zone is interpreted as a domain of consolidated powder because consolidation is accompanied with both shrinkage leading to the surface depression and elimination of light-scattering interfaces. Viscous merging of softened powder particles is supposed to be the principal mechanism of consolidation. Mathematical model based on this mechanism confirms formation of the consolidated zone in the center. Both the experiment and the model indicate that consolidation looks like propagation of sharp front. The calculated diameter of the consolidated zone underestimates the experimentally observed one. The discrepancy can be explained by the uncertainty in the high-temperature viscosity of silica glass. Comparison of the experiments and the calculations estimates the temperature of the consolidation front of about 1800-1900 K. Coloring of the sample surface with ink visualizes zones of lower temperature around the consolidated powder.

Acknowledgements

This work has been financed by the Ministry of Education and Science of the Russian Federation (grant agreement № 14.574.21.0079 from 08.07.2014, project id: RFMEFI57414X0079).

References

Deckers, J., Meyers, S., Kruth, J.-P., Vleugels, J., 2014. Direct selective laser sintering/melting of high density alumina powder layers at elevated temperatures. Phys. Procedia 56, 117.

Gusarov, A.V., Kovalev, E.P., 2009. Model of thermal conductivity in powder beds, Phys. Rev. B 80, 024202.

Gusarov, A.V., Pavlov, M., Smurov, I., 2011. Residual stresses at laser surface remelting and additive manufacturing. Phys. Procedia 12, 248.

Gusarov, A.V., Malakhova-Ziablova, I.S., Pavlov, M.D., 2013. Thermoelastic residual stresses and deformations at laser treatment. Phys. Procedia 41, 889.

JANAF, 2016. Thermochemical tables, (http://kinetics.nist.gov/janaf/).

Khmyrov, R.S., Grigoriev, S.N., Okunkova, A.A., Gusarov, A.V., 2014. On the possibility of selective laser melting of quartz glass, Phys. Procedia 56, 345.

Khmyrov, R.S., Protasov, C.E., Grigoriev, S.N., Gusarov, A.V., 2016. Crack-free selective laser melting of silica glass: single beads and monolayers on the substrate of the same material. Int. J. Adv. Manuf. Technol. DOI 10.1007/s00170-015-8051-9.

Kingery, W.D., 1960. *Introduction to ceramics*, Wiley, New York.

Li, Q., Danlos, Y., Song, B., Zhang, B., Yin, S., Liao, H., 2014. Effect of high-temperature preheating on the selective laser melting of yttria-stabilized zirconia ceramic. J. Mater. Process. Technol. 222, 61.

Okunkova, A., Volosova, M., Peretyagin, P., Vladimirov, Yu., Zhirnov, I., Gusarov, A.V., 2014. Experimental approbation of selective laser melting of powders by the use of non-Gaussian power density distributions. Phys. Procedia 56, 48.

Richter, F., 2006. *Upsetting and Viscoelasticity of Vitreous SiO2: Experiments, Interpretation and Simulation. Thesis.* Technical University of Berlin.

Tang, H.H., Liu, F.H., Lin, W.H., 2006. Rapid prototyping machine based on ceramic laser fusion. Int. J. Adv. Manuf. Technol. 30, 687.